THE EJECTION-SWEEP CHARACTER OF SCALAR FLUXES IN THE UNSTABLE SURFACE LAYER

GABRIEL KATUL[1,2], GREG KUHN[1], JOHN SCHIELDGE[3] and CHENG-I HSIEH[1]
[1]*School of the Environment, Box 90328, Duke University, Durham, NC 27708-0328, U.S.A.;* [2]*Center for Hydrologic Sciences, Duke University, Durham, NC 27708-0230, U.S.A.; and* [3]*Jet Propulsion Laboratory, California Institute of Technology, Pasadena, CA 91109-8099, U.S.A.*

(Received in final form 18 July, 1996)

Abstract. In the atmospheric surface layer, it is widely accepted that ejection and sweep eddy motions, typically associated with coherent structures, are responsible for much of the land-surface evaporation, sensible heat, and momentum fluxes. The present study analyzes the ejection-sweep properties using velocity and scalar fluctuation measurements over tall natural grass and bare soil surfaces. It is shown that momentum ejections and sweeps occur at equal frequencies ($D_{\text{eject}} \approx D_{\text{sweep}} \approx 0.29$) irrespective of surface roughness length or atmospheric stability conditions. Also, their magnitudes are comparable to values reported from open channel velocity measurements ($D_{\text{sweep}} \approx 0.33$; $D_{\text{eject}} \approx 0.30$). The scalar D_{eject} is constant and similar in magnitude to the momentum $D_{\text{eject}}(\approx 0.29)$ over both surfaces and for a wide range of atmospheric stability conditions, in contrast to the scalar D_{sweep}. The scalar sweep frequency is shown to depend on the scalar skewness for the dynamic convective and free convective sublayers, but is identical to D_{eject} for the dynamic sublayer. The threshold scalar skewness at which the D_{sweep} dependence occurs is 0.25, in agreement with the accepted temperature skewness value at near-neutral conditions. In contrast to a previous surface-layer experiment, this investigation demonstrates that the third-order cumulant expansion method (CEM) reproduces the measured relative flux contribution of ejections and sweeps (ΔS_0) for momentum and scalars at both sites. Furthermore, a linkage between ΔS_0 and the scalar variance budget is derived via the third-order CEM in analogy to momentum. It is shown that ΔS_0 can be related to the flux divergence term and that such a relationship can be estimated from surface-layer similarity theory, and the three sublayer model of Kader and Yaglom and proposed similarity functions.

1. Introduction

Coherent structures near rough and smooth boundaries have been the subject of theoretical and experimental research for the past two and half decades and continue to be a central research topic in momentum, heat, and mass transport (see e.g. Kovasznay et al., 1970; Raupach and Thom, 1981; Raupach et al., 1991). In boundary-layer turbulence, it is now recognized that downdrafts (or sweeps) and updrafts (or ejections) are the primary constitutive motions of such coherent structures. Hence, interest in the properties of these two types of eddy motions has been the subject of extensive research (see Cantwell, 1981; Robinson, 1991, for reviews).

For rough surfaces, experiments in the laboratory demonstrated the dominant role of downdrafts relative to updrafts in transporting momentum in the near-wall region, while a balance between these two mechanisms appears to exist in the 'equilibrium region' of many laboratory flows. Furthermore, the statistical properties of these two mechanisms in the equilibrium region appear to be independent of the

Boundary-Layer Meteorology **83:** 1–26, 1997.

wall-roughness as speculated by Townsend (1976) and demonstrated by Raupach (1981) using wind-tunnel experiments and Nakagawa and Nezu (1977) using open channel measurements.

Krogstad et al. (1992) re-evaluated the roughness-independence in the equilibrium region using wind-tunnel velocity measurements above rough and smooth boundaries. Their measurements indicated that over the rough surface, both ejection and sweep frequencies were twice those measured over a smooth surface. Also, the reported spectra from the same experiment demonstrated that the strength of 'active' motion in the outer layer clearly depends on surface roughness. This result directly conflicts with Townsend's (1976) 'rough-wall similarity hypothesis', and to some extent, Monin and Obukhov's (1954) similarity theory (MOST), which states that outside the roughness sublayer (a region influenced by length scales associated with the roughness elements), turbulent motion is strictly independent of the boundary roughness except through its influence on the friction velocity (u_*).

While the ejection-sweep duration, frequency, and stress contribution for the equilibrium region over rough and smooth boundary layers continues to be the subject of research in momentum transport, less attention has been devoted to scalar transport. We note that if Townsend's hypothesis is extended to the scalar fluctuations, then the turbulent scalar transport must be independent of the surface properties except through the scalar flux in analogy to momentum.

Laboratory scalar experiments analogous to Krogstad et al. (1992) are less numerous than their momentum counterpart, but the outcome of a wide range of atmospheric surface layer (ASL) experiments above uniform and non-uniform terrain types can provide qualitative assessments to Townsend's hypothesis for heat transport.

For example, many experiments that evaluated the so called 'flux-variance' method (see Tillman, 1972; Wesely, 1988; Lloyd et al., 1991; Padro, 1993; De Bruin et al., 1991, 1993; Albertson et al., 1995; Katul et al., 1995, for reviews) suggested that (1) heat and water source-sink non-uniformity can alter the dimensionless scalar variance similarity constants at measurement heights well above four times the canopy height (h), and (2) that the correlation coefficient between heat and water vapour turbulent fluctuations is different from unity in the ASL. Both of these findings for scalar transport in the ASL parallel Krogstad et al.'s (1992) argument for momentum since it is evident that scalar source variability at the ground surface influences the statistical structure of the ASL, as was noted for the roughness variability. In fact, Weaver's (1990) conclusion regarding calibration of the flux-variance method for determining ASL fluxes clearly points out the need for varying the similarity constants depending on terrain type.

Roughness sublayer (RSL), canopy sublayer (CSL), and ASL experiments that considered the ejection-sweep relationship for scalar and momentum transport also provide conflicting views (see Finnigan, 1985; Figure 3 for a schematic definition of RSL, CSL, and ASL). Coppin et al.'s (1986) pioneering laboratory experiment on heat dispersion using a planar heat source within a model canopy utilized quadrant

analysis of vertical heat flux and showed that sweeps and ejections contribute equally to the heat flux close to the canopy height (h). However, for large heat flux excursions at this height, sweeps were clearly dominant in analogy to momentum. Based on this analogy, Coppin et al. (1986) concluded that heat and momentum transport are similar as long as the scalar source and momentum sink distributions are 'roughly' coincident, as they often are in real canopies. Another interesting finding in the Coppin et al. (1986) heat dispersion experiment is that ejections close to the canopy surface depend on height above the ground surface (z), while sweeps are independent of z. Chen's (1990) experiment above rough mallee bushland revealed that sweeps and ejections were in near-equilibrium for heat and momentum in the neutral ASL. For the unstable ASL, large excursions in momentum and heat fluxes appear to be dominated by sweeps and ejections respectively, which is not consistent with Maitani and Ohtaki (1987) who found that ejections transport both heat and momentum more efficiently in the unstable ASL above bare soil and water. Also, in contrast to momentum fluxes, Chen's (1990) measurements show that the relative contribution of sweeps and ejections to ASL heat transport depends on atmospheric stability. Based on these findings, Chen (1990) concluded that the mechanisms for momentum and heat transport are different even at heights as large as $4h$. Furthermore, Chen's (1990) calculation of the differential contribution to scalar flux from sweeps and ejections (ΔS_0) by a third order cumulant expansion method (CEM) underpredicted the eddy correlation measured ΔS_0 by a factor of 8. However, from the same experiment, the CEM-predicted ΔS_0 reproduced the measured ΔS_0 well for momentum in agreement with earlier ASL and RSL studies (e.g. Shaw et al., 1983). Chen (1990) attributed the discrepancy between measured and CEM-predicted ΔS_0 for heat and momentum to dissimilarity in their transport mechanisms. Table I summarizes relevant results from other ASL, RSL, and CSL experiments that analyzed the ejection-sweep character of turbulence.

It is the conclusions regarding the influence of roughness in Krogstad et al. (1992), the potential limitations of Townsend's wall similarity hypothesis to ASL scalar transport, and the need to link the ASL ejection-sweep character (i.e. time fraction of occurrence and turbulent flux contribution) to prognostic equations such as the scalar variance budget that have motivated this study.

The third-order CEM, originally proposed by Frenkiel and Klebanoff (1967; 1973) and Antonia and Atkinson (1973), is utilized. We focus on the third order CEM only because of potential linkages between third-order cumulants, ejections and sweeps, and the turbulent kinetic energy (TKE) transport term as discussed in Nakagawa and Nezu (1977). Furthermore, the third-order CEM was validated by Shaw et al. (1983) and Raupach (1981) for momentum. However, as noted above, Chen's (1990; Figure 14) measurements suggest that the third-order CEM predictions of ΔS_0 for scalar fluxes underestimate the measurements by a factor of 8. Nagano and Tagawa (1988) showed that a fourth-order CEM reproduced all the third-order scalar and mixed velocity-scalar statistics in both the inner and outer region of turbulent air flow in a heated pipe. This discrepancy in CEM performance

Table I

Summary conclusions of some atmospheric surface layer (ASL), roughness sublayer (RSL), and canopy sublayer (CSL) experiments related to the ejection-sweep character of turbulence. Many more experiments were performed but are not included in Table I

Authors	Surface	Comments
Bergstrom and Hogstrom (1989)	Pine Forest	Dissimilarity in the ejection-sweep contribution to heat, water vapor, and momentum turbulent fluxes. Specifically, the measured ejection contribution to the scalar fluxes of heat and water vapor was larger than the sweep contribution even at $z = 2.36h$. Atmospheric stability effects were not considered.
Coppin et al. (1986)	Wind Tunnel (heated elements)	CSL and RSL heat and momentum transport are similar as long as the scalar source and momentum sink distributions 'roughly' coincide.
Maitani and Shaw (1990)	Deciduous Forest	Relative contributions to sensible heat flux by sweeps were significantly larger than those by updrafts for RSL and CSL, while in the ASL the relative ejection contributions were slightly larger than those by sweeps. Atmospheric stability effects were not considered.
Maitani and Ohtaki (1987)	Rice paddy, bare soil, and water surfaces	Sweeps were more efficient than ejections in transporting heat and momentum for near-neutral conditions in the RSL. However, ejections became more efficient than sweeps for heat transport under very unstable conditions.
Nakagawa and Nezu (1977)	Open channel, smooth and rough	In the equilibrium region, a near-balance exists between ejection and sweep contribution to momentum.
Raupach (1981)	Wind tunnel, smooth and rough	Sweep and ejection contribution to the momentum flux are in balance and are independent of surface roughness in the equilibrium region.
Shaw et al. (1983) and Shaw (1985)	Corn and wheat	Sweeps marginally exceed ejections for momentum at z/h = 1.6 (transition between RSL and ASL).

for momentum and scalar fluxes motivated us to further investigate the third-order CEM approximation.

In this study, we utilize data sets from two ASL experiments. In the first experiment, 10 Hz velocity (U_i), air temperature (T_a), and water vapour concentration (Q) measurements were collected at z = 2.65 m for 5 days in October of 1994 within a grass-covered forest clearing (grass height h = 50 cm) in Durham, North Carolina. In the second experiment, 21 Hz U_i and T_a measurements were collected at z = 1.96 m for three days above a uniform bare soil surface prior to and following an irrigation event in August 1993 (see Katul et al., 1994a,b). The estimated momentum roughness heights (z_0) for bare soil and grass were 2 mm and 4 to 10 cm respectively.

The notation used throughout this study is as follows: U_i ($U_1 = U$, $U_2 = V$, $U_3 = W$) are the instantaneous longitudinal (U), lateral (V), and vertical (W)

velocity components, x_i (x_1, x_2, x_3) are the longitudinal (x), lateral (y), and vertical (z) directions, z is defined from the ground surface, $\langle\ \ \rangle$ is the time averaging operator assumed to converge to ensemble averaging by the ergodic hypothesis (Monin and Yaglom, 1971 pp. 214–218); u_i, T, and q are the turbulent fluctuations of velocity, air temperature, and water vapour concentration about time averages with $\langle u_i \rangle = \langle T \rangle = \langle q \rangle = 0$; and the x direction is aligned along the mean horizontal wind so that $\langle V \rangle = 0$.

2. Experimental Setup

2.1. GRASS-COVERED FOREST CLEARING

The first experiment was conducted in October 1994 at the Blackwood Division of the Duke Forest in Durham, North Carolina from Day of Year (DOY) 297 to 301. The site is a grass-covered clearing surrounded by a uniform 10–13 m tall Loblolly pine forest. Two unpaved roads bounded the western and northern edges of the 480 m long (north-south direction) and 305 m wide (east to west) forest clearing. The surface cover consisted of a mixture of dry and green *Alta Fescue* grasses ranging in height from 20–100 cm. While the typical grass height was 40 cm over most of the field, tall dry grasses predominated on the northern and southern borders of the field and in a patch just east of the centre. The height of green grasses increased from 40–100 cm in a direction west-northwest from the center of the field. At the center of the clearing, the mean grass height (h) was 50 cm.

During the study period, two frontal passages occurred on Days 296 and 299. Sky conditions varied from clear to overcast. Near-surface air temperatures fell below freezing in the morning on a few days and frost was sometimes noticeable on the grass just after sunrise. Occasional measurements with a portable quick draw tensiometer indicated that maximum moisture content occurred near the center of the field and a marginal but persistent decrease along the transect toward the north was documented. This observation was further supported by surface temperature measurements taken with a Raytek hand held infrared radiometer (IRR) that showed an increase in average surface temperature from the centre to the northern edge of the field.

The eddy correlation instruments, consisting of a Campbell Scientific Krypton (KH2O) hygrometer co-located with a 3-axis Gill anemometer, were positioned at a central mast, 200 m from the northern edge at z = 2.65 m (i.e. z/h = 5.2). We note that Garratt (1978) and Chen (1990) both found the onset of the lower ASL limit for heat and momentum to be at $z/h = 4$. The Gill anemometer details can be found in Katul et al. (1994a,b). All instruments were aligned to point north prior to the experiment. The U, V, W, T, and Q were sampled at 10 Hz and segmented into runs for which the sampling duration per run (T_p) was 27.3 minutes. Hence,

16,384 measurements per flow variable were sampled per run. The analog signals from all instruments were sampled by a 21X Campbell Scientific micrologger and transferred to the hard drive of a personal computer via an optically isolated RS232 interface for future processing. The raw data for each run were transformed so that the mean longitudinal velocity $\langle U \rangle$ was aligned along the mean horizontal wind direction and $\langle V \rangle = \langle W \rangle = 0$. The data collection started around 0800 LT and was terminated about 1800 LT. The amount of data collected each day varied from 8 to 28 runs depending on weather conditions. Time series were inspected to identify and exclude runs without constant mean temperature and water vapour concentrations. This screening resulted in 41 runs. For these runs, the u_* and sensible heat flux (H) varied between 0.17 to 0.44 m s^{-1} and 5 to 180 W m^{-2} respectively. To estimate z_0, we measured $\langle U \rangle$ and $u_* (= [-\langle uw \rangle]^{1/2})$ for near-neutral runs. The z_0 values were dependent on wind direction and varied from 4–10 cm, which is consistent with the reported values in the literature (Sorbjan, 1989 p. 68).

2.2. UNIFORM BARE SOIL

The data used in the second experiment were collected at the Campbell Tract facility located at the University of California in Davis. The site is a 500 m by 500 m tract of uniform Yolo clay loam equipped with a sprinkler irrigation system. The measurements were conducted in August, 1993 prior to and following irrigation. A Gill triaxial sonic anemometer that was set at $z = 1.96$ m was used to measure U_i and T_a. We chose this height as a compromise between our ability to sample turbulence influenced by the irrigated source area and our need to resolve at least one decade of inertial subrange scales. The sampling frequency and period were 21 Hz and 26 min, respectively, resulting in 32,768 data points per flow variable. We note that for such sampling frequencies and measurement heights, some high frequency contributions may not be adequately resolved by the sonic anemometer. However, since the objective of this study is to investigate the statistical properties of the ejection-sweep cycle, the role of such high frequency events is of minor importance when compared to the more coherent large-scale events. The momentum roughness length was estimated at 2 mm from another experiment (see Katul et al., 1994 a,b). At this site, 34 runs were used of which 16 runs were collected just after a 10 h irrigation on the evening of DOY 233. For these 33 runs, the u_* and H ranges were 0.03 to 0.36 m s^{-1} and 2 to 332 W m^{-2} respectively. Details regarding the experimental setup at the Davis bare soil site can be found in Katul et al. (1994a,b) and regarding the irrigation system and other site information in Katul and Parlange (1992, 1994).

Both surfaces were hydrodynamically rough since the minimum measured roughness Reynolds number $z_+ (= u_* z_0 / \nu \approx 13)$ exceeded 2 for all runs, where ν is the air kinematic viscosity (see Brutsaert, 1982, p. 92; Monin and Yaglom, 1971, p. 289). To compare with laboratory experiments, it is necessary to distinguish whether the surface roughness is 'k-type' (irregular corrugations and proturbances)

or 'd-type' (regular corrugations with very unstable flow around them) as discussed in Perry et al. (1969). For both experiments, the surfaces are considered 'k-type' rather than 'd-type'. The distinction between 'k-type' and 'd-type' roughness and its implication on the ejections-sweep cycle in the roughness sublayer is discussed in Townsend (1976, pp. 140–142). Further details about the experimental setup and the onset of the inertial layer, estimated from a balance between turbulent production and dissipation, can be found in Hsieh et al. (1996).

3. Methods of Analysis

The contribution of the ejection-sweep cycle to momentum and scalar fluxes is quantified by the conditional sampling methods reviewed in Antonia (1981) and Bogard and Tiederman (1987). For completeness, a summary of these analyzing methods is presented.

Quadrant analysis refers to a set of analyzing techniques that are applied to scatter plots formed by two turbulent quantities such as vertical velocity fluctuations (w) and a flow variable (c) fluctuation (e.g., u_1, T, and q). In analogy to momentum transport, four quadrants defined by the Cartesian axes of the scatter plot (S_i, $i = 1, \ldots, 4$) are used to represent four modes of turbulent transport: (e.g., $w > 0$ and $c > 0$, $w < 0$ and $c > 0$, $w > 0$ and $c < 0$, and $w < 0$ and $c < 0$). The quadrant nomenclature for scalar and momentum transport is presented in Figure 1, where the nomenclature for momentum and scalars are identical to those used by Willmarth and Lu (1974) and Chen (1990) respectively. That is, quadrants 4 and 1 define ejection events, and quadrants 2 and 3 define sweep events, for momentum and scalar fluxes respectively.

The stress fraction S_i for quadrant 'i' is defined as the flux contribution to wc from that quadrant using

$$S_i = \frac{\langle\langle wc\rangle\rangle_i}{\langle wc\rangle}, \qquad \langle\langle wc\rangle\rangle_i = \frac{1}{T_p}\int_0^{T_p} w(t)c(t)I_i \,\mathrm{d}t, \tag{1}$$

where $\langle\langle \quad \rangle\rangle$ are conditional averages, I_i is the indicator function defined by

$$I_i = \left\{ \begin{array}{ll} 1 & \text{if event coordinates } (w, c) \text{ are within quadrant } i;\ i = 1, 2, 3, 4 \\ 0 & \text{otherwise,} \end{array} \right\} \tag{2}$$

with $S_1 + S_2 + S_3 + S_4 = 1$. As discussed in Subramanian et al. (1982), the above approach is ill suited for constructing ensemble structural ejection-sweep elements but is reliable in producing conditional averages influenced by ejections and sweeps.

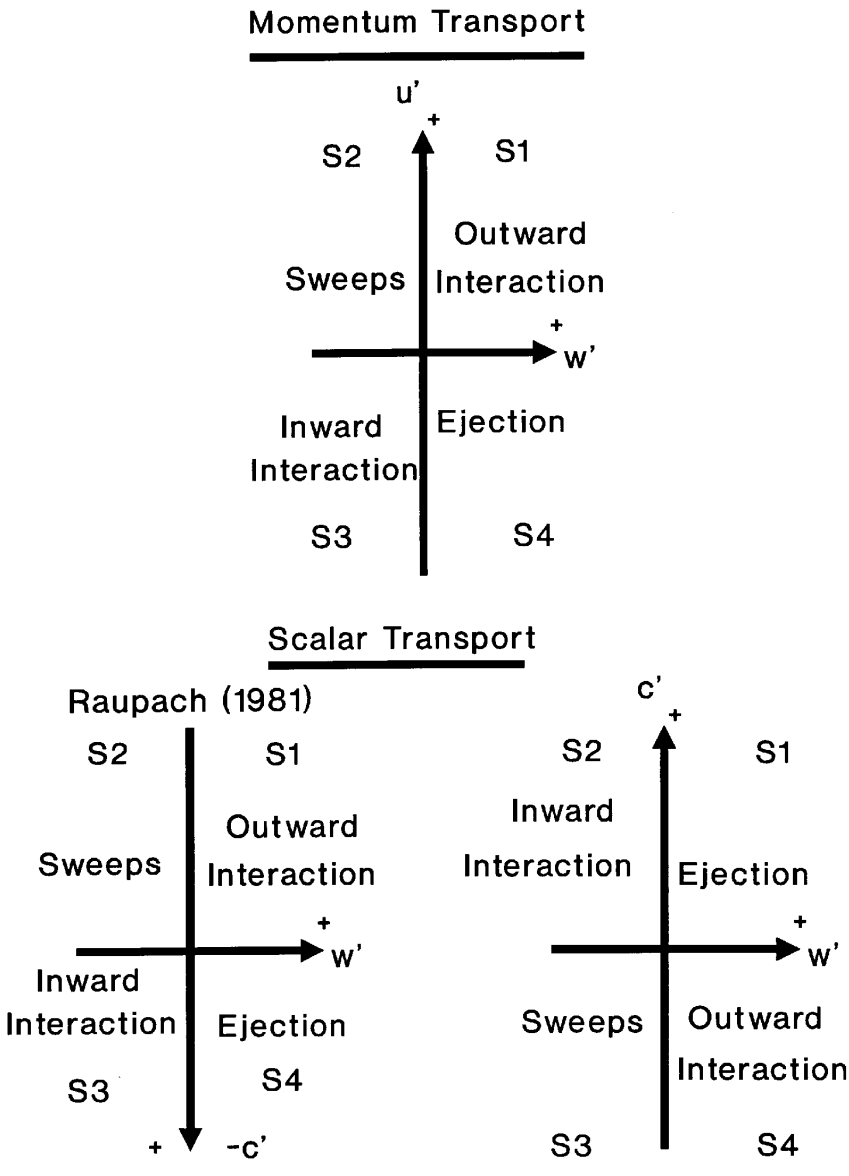

Figure 1. Ejection-sweep definitions for scalar and momentum transport. Events in quadrants 2 and 4 define sweeps and ejections for momentum fluxes, respectively. Events in quadrants 3 and 1 define sweeps and ejections for scalar fluxes, respectively. A coordinate transformation can be applied to the scalar time series so that quadrants 2 and 4 define sweeps and ejections as necessary to the application of Raupach (1981) result (see Equation (3)) rather than quadrants 3 and 1.

Based on a third-order CEM, Nakagawa and Nem (1977) and Raupach (1981) showed that the difference between stress fractions due to sweeps and ejections

($\Delta S_0 = S_4 - S_2$), which is a measure of the relative importance of the two types of mechanisms, is given by

$$\Delta S_0 = \frac{R_{wc}+1}{R_{wc}\sqrt{2\pi}}\left(\frac{2C_1}{(1+R_{wc})^2}+\frac{C_2}{1+R_{wc}}\right),$$

$$C_1 = (1+R_{wc})\left(\frac{1}{6}(M_{03}-M_{30})+\frac{1}{2}(M_{21}-M_{12})\right), \tag{3}$$

$$C_2 = -\left(\frac{1}{6}(2-R_{wc})(M_{03}-M_{30})+\frac{1}{2}(M_{21}-M_{12})\right),$$

where R_{wc} is the correlation coefficient given by

$$R_{wc} = \frac{\langle wc\rangle}{\sigma_w \sigma_c}, \tag{4}$$

and M_{ij} are the dimensionless joint moments given by

$$M_{ij} = \frac{\langle w^i c^j\rangle}{(\sigma_w)^i(\sigma_c)^j}, \tag{5}$$

where $\sigma_c = \langle c^2\rangle^{1/2}$ and $\sigma_w = \langle w^2\rangle^{1/2}$ are the standard deviations of c and w, respectively ($c = u, T, q$), and $M_{11} = R_{wc}$. The durations of ejections and sweeps are given by

$$D_i = \frac{1}{T_p}\int_0^{T_p} I_i(t)\,\mathrm{d}t, \tag{6}$$

where D_1 and D_4 are total ejection, and D_3 and D_2 are total sweep, durations in T_p for scalar and momentum transport respectively (see Figure 1). Also, D_i can be viewed as the ratio of the total duration of events in quadrant i to the sampling period T_p. Therefore, D_i is the time fraction of measurement events in quadrant i (hereafter referred to as time fraction in keeping with Coppin et al., 1986).

4. Results and Discussion

We present the results in two subsections. In the first subsection, similarity between the ejection-sweep character of momentum and scalar transport in the ASL is considered at both sites. The second subsection explores the linkages between ΔS_0 and scalar variance budgets using the CEM approach. Validations of the CEM approach for scalar transport are also discussed.

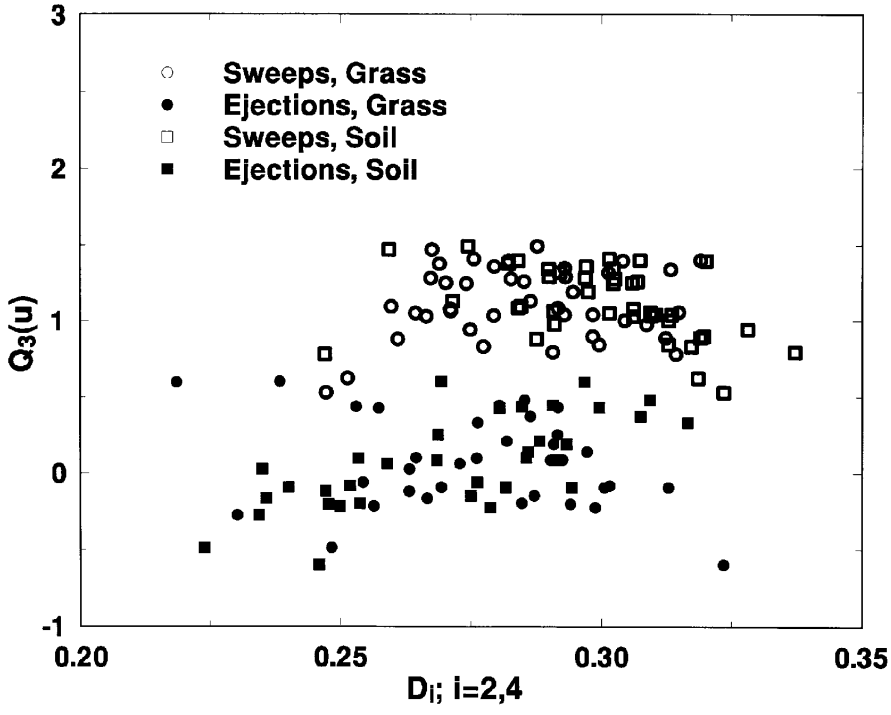

Figure 2a.

Figure 2. The variation of skewness Q_3 of c with ejections (D_{eject}) and sweeps (D_{sweep}) time fraction for all runs: (a) c = longitudinal velocity (u), (b) c = temperature (T) and water vapour concentration (q).

4.1. ASL EJECTION-SWEEP CHARACTER FOR MOMENTUM AND SCALARS

Raupach (1981), Maitani and Ohtaki (1987) and Nagano and Tagawa (1988) demonstrated that the skewness is sensitive to the ejection-sweep occurrence and turbulent flux contribution. Hence, in Figures 2a and 2b, the sweep and ejection (D_{sweep} and D_{eject}) frequencies for each run are shown as a function of the skewness ($Q_3 = \langle c^3 \rangle / \sigma_c^3$) for $c = u$, T, and q.

It is evident from Figure 2 that the ejection-sweep momentum time fraction at both sites is nearly constant and does not vary with the longitudinal velocity skewness. In contrast to the momentum ejection time fraction, the scalar sweep time fraction varies with skewness, especially at the bare soil site. Therefore, our analysis indicates that the relationship between sweep time fraction and skewness for heat (see Figure 2b) is not identical to its momentum counterpart (see Figure 2a) for strongly unstable conditions (large temperature skewness).

From Figure 2a, notice that the momentum D_{sweep} and D_{eject} are not sensitive to variations in z_0 as well. We compared our measured D_{sweep} and D_{eject} at both sites with the mean $D_{\text{sweep}} (= 0.33)$ and the mean $D_{\text{eject}} (= 0.30)$ reported by Nakagawa

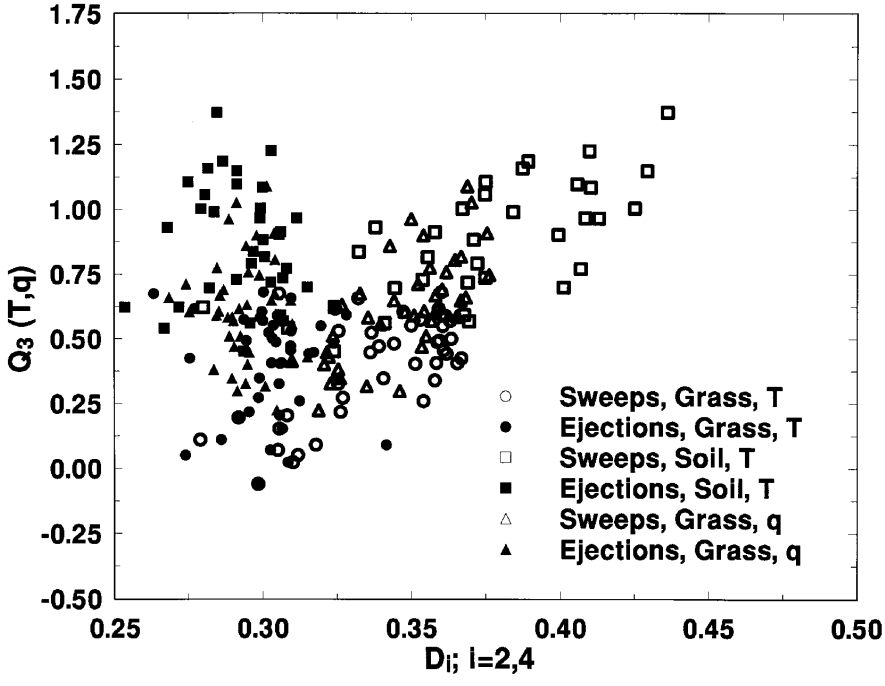

Figure 2b.

Table II

Comparison between the ejection/sweep frequencies $(D_{\text{eject}}/D_{\text{sweep}})$ for heat and momentum at both sites. The open channel (water) values are for rough and smooth boundaries obtained by depth averaging the measurements reported in Nakagawa and Nezu (1977) for the inertial sublayer. The open channel (oil) are from Brodkey et al. (1974) for a wall distance $y^+ > 30$. The numbers in brackets are the standard deviations about the mean

Flux	Sweeps/ ejections	Grass (z_0 = 4–10 cm)	Bare soil ($z_0 = 0.2$ cm)	Channel (oil)	Channel (water)
Momentum	D_{sweep}	0.29 (0.018)	0.28 (0.022)	0.30	0.33
	D_{eject}	0.30 (0.018)	0.27 (0.024)	0.28	0.30
Heat	D_{sweep}	0.34 (0.024)	0.37 (0.036)	***	***
	D_{eject}	0.30 (0.015)	0.29 (0.014)	***	***
Water vapor	D_{sweep}	0.35 (0.018)	***	***	***
	D_{eject}	0.29 (0.010)	***	***	***

and Nezu (1977) for smooth and rough open channel flows (see Table II). While D_{eject} is in good agreement with the value in Nakagawa and Nezu (1977), D_{sweep} systematically underpredicted their reported value. However, our D_{sweep} and D_{eject} measurements agree better with Brodkey et al. (1974) for $y^+ (= u_* z/\nu) > 30$.

While some differences between D_{eject} and D_{sweep} exist, Figure 2a does not strictly support the conclusions in Krogstad et al. (1992). If Krogstad et al.'s (1992) conclusions are extended to our study, then D_{eject} and D_{sweep} should depart appreciably since the roughness length changed by a factor of 10. Hence, it is unclear why our results and those of Raupach (1981) are at variance with the Krogstad et al. (1992) conclusions. Recall that the study by Krogstad et al. (1992) demonstrated that S_2 and hence ΔS_0 is dependent on z_0, and this dependence persisted in the equilibrium layer.

For the neutral ASL, it is recognized that similarity in the turbulence statistics exists independent of the external flow conditions (e.g. surface roughness). This near-neutral ASL property is evident from the measured σ_w/u_*, σ_u/u_*, and M_{03} that appear to be independent of z_0 for a wide range of z_0 values (see Panofsky and Dutton, 1984). Hence, Krogstad et al.'s (1992) conclusions are not consistent with many ASL experiments. This inconsistency suggests that the Krogstad et al. (1992) experiment is not representative of the ASL and we consider this point next. Notice that the wind-tunnel velocity data in Raupach (1981; Figure 9) display an average $\Delta S_0 \approx +0.05$ for z/δ = 0.1–0.2, where δ is the height of the boundary layer. For this z/δ range, Raupach's (1981; Figure 1) data show that σ_u/u_* and σ_w/u_* are also constant independent of z or z_0. Krogstad et al.'s (1992) experiment shows that for z/δ = 0.1–0.2, ΔS_0 ranges from +0.01 to +0.05 depending on the surface roughness. We chose this z/δ range since this height range is comparable with the ASL definition within the atmospheric boundary layer (ABL). For $0.15 < z/\delta < 0.4$ however, ΔS_0 = +0.05 for all roughness conditions in Krogstad et al. (1992) and is not different from the value reported in Raupach's (1981) experiment. It appears that the roughness sublayer in Krogstad et al. (1992) may have been larger than in Raupach (1981). As for the spectral differences reported in their Figure 12, we can only question their experimental setup in relation to restricted lateral velocity fluctuations due to the small tunnel width (b). This lateral restriction is absent in the ASL, and minor in Raupach's (1981) wind-tunnel experiment. To illustrate this possible lateral restriction in Krogstad et al. (1992), we consider the ratio σ_v/σ_u in relation to δ/b. The ratio σ_v/σ_u measures the dampening of the lateral velocity fluctuations as restricted by tunnel side walls relative to the longitudinal velocity fluctuations, while δ/b is a geometric measure of the restriction. In the ASL, the planar width is much larger than the ABL height so that $\delta/b \approx 0$. However, in laboratory experiments, δ/b is finite and varies with the experimental setup. Our ASL measurements resulted in a mean $\sigma_v/\sigma_u \approx 0.97$ for unstable and near-neutral stability conditions. In Raupach's (1981) wind-tunnel data (width b = 1330 mm, $\delta \approx$ 100 mm; δ/b = 0.075), σ_v/σ_u varied from 0.4–0.6 for z/δ = 0.1–0.2. Notice that less than an 8% restriction (measured by δ/b) reduced σ_v/σ_u by a factor of 2 relative to the ASL data. In Krogstad et al.'s (1992) wind-tunnel experiment, σ_v was not reported but the dimensions of the wind tunnel at the working section are b = 152 mm, $\delta \approx$ 75 mm, and $\delta/b = 0.5 \gg 0.075$ reported by Raupach (1981). Clearly, with such lateral restrictions, $\sigma_v/\sigma_u \ll 1$ for Krogstad et al.'s (1992) data,

and this experiment may not represent the three-dimensional turbulent structure of the ASL.

In contrast to momentum transport, Figure 2b shows that the imbalance between D_{sweep} and D_{eject} increases with increasing Q_3 for both T and q. Hence, notice that D_{sweep} depends on external conditions (e.g. z/L_{mo}) while D_{eject} appears constant independent of z_0. Also, D_{eject} for scalar transport is nearly identical to D_{eject} for momentum transport.

Here, L_{mo} is the Obukhov length given by

$$L_{mo} = -\frac{\rho_a u_*^3}{kg\left(\dfrac{\langle wT\rangle}{\langle T_a\rangle} + 0.61\langle wq\rangle\right)}, \tag{7}$$

where $k = 0.4$ (Von Karman's constant), g is the gravitational acceleration, and ρ_a is the air density. The stability parameter $\chi = -z/L_{mo}$ for this experiment (75 runs) was used to classify the runs. The following stability range distribution was obtained: $0 < \chi < 0.2$ (8 runs), $0.2 < \chi < 2$ (62 runs), $\chi > 2$ (5 runs). These stability ranges roughly correspond to the dynamic, dynamic-convective, and free-convective sublayers respectively (see Katul et al., 1996).

The sensitivity of D_{sweep} to the scalar skewness suggests dissimilarity between momentum and scalar transport when the scalar skewness exceeds 0.25 (see Figure 2b). For a scalar skewness not exceeding 0.25, D_{sweep} and D_{eject} have values comparable to their momentum counterpart. Interestingly, Raupach and Thom (1981) proposed a velocity skewness of +0.2 for defining the upper limit of the RSL that is in good agreement with the skewness value at which scalar ejections and sweeps become dissimilar in Figure 2b. Also, their 0.2 skewness value is consistent with Wyngaard and Sundarajan's (1977, Figure 1) temperature skewness value for a near-neutral ASL. This similarity between scalar and momentum transport for near-neutral conditions is also in agreement with Chen's (1990) conclusions.

While Figures 2a and 2b demonstrate similarities in the ejection frequencies, and dissimilarities between momentum and scalar sweep frequencies, it is not clear whether these departures are responsible for the apparent failure of the third-order CEM for scalar transport as concluded by Chen (1990). Therefore, we consider next whether the measured ΔS_0 for scalar fluxes can be reproduced from a third-order CEM.

4.2. THIRD-ORDER CUMULANT EXPANSION METHOD FOR PREDICTING ΔS_0

In Figures 3a and 3b, the predicted ΔS_0 from Equation (3) is compared with the measured ΔS_0 obtained from quadrant analysis for momentum and scalar fluxes respectively. In Equation (3), the eddy-correlation measured R_{wc} and M_{ij} were used for $c = u$, T, and q. The predicted ΔS_0 from (3) is in excellent agreement with the measured ΔS_0 for momentum, heat, and water vapour. It is unclear to us why our results are at variance with Chen (1990). We postulate that Chen's

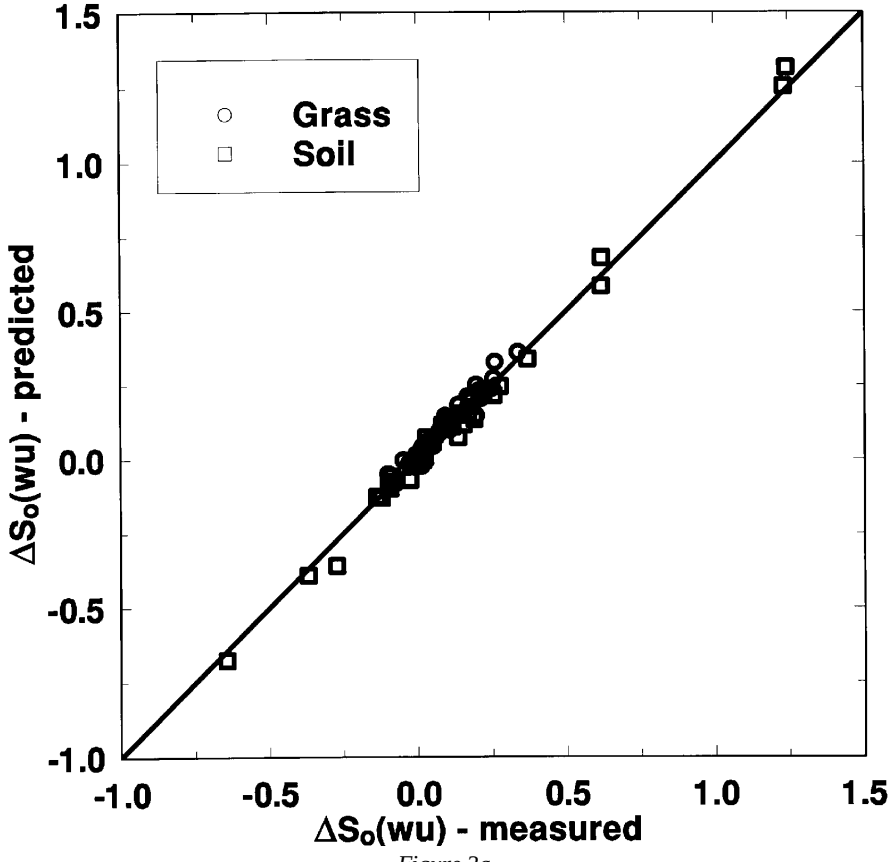

Figure 3a.

Figure 3. A comparison between measured and third-order cumulant discard predicted ΔS_0: (a) for momentum, (b) for heat and water vapor and all runs. The 1 : 1 line is also shown.

(1990) calculations did not account for the fact that the original cumulant discard approximation in Nakagawa and Nezu (1977) is derived for quadrants 2 and 4 and is not appropriate for quadrants 1 and 3 (as evidenced by their sign convention). However, for scalar transport, Equation (3) can still be used if the T and q time series are multiplied by -1. This operation transforms quadrants 1 and 3 to quadrants 2 and 4 (see Figure 1) without requiring a separate derivation for a scalar flux ΔS_0 (although it is possible to derive such a relationship using the method discussed in Nagano and Tagawa, 1988, 1990 by truncating after third cumulants).

Care should be exercised when interpreting the results in Figure 3a because, (1) ΔS_0 is computed by differencing fluxes in quadrants 2 and 4, which results in an error cancellation effect (the same measurement error contributes to $\langle\langle wc\rangle\rangle_2$ and $\langle\langle wc\rangle\rangle_4$), and (2) the comparison between measured and predicted ΔS_0 using Equation (3) is somewhat biased by the fact that R_{wc} is used in normalizing the

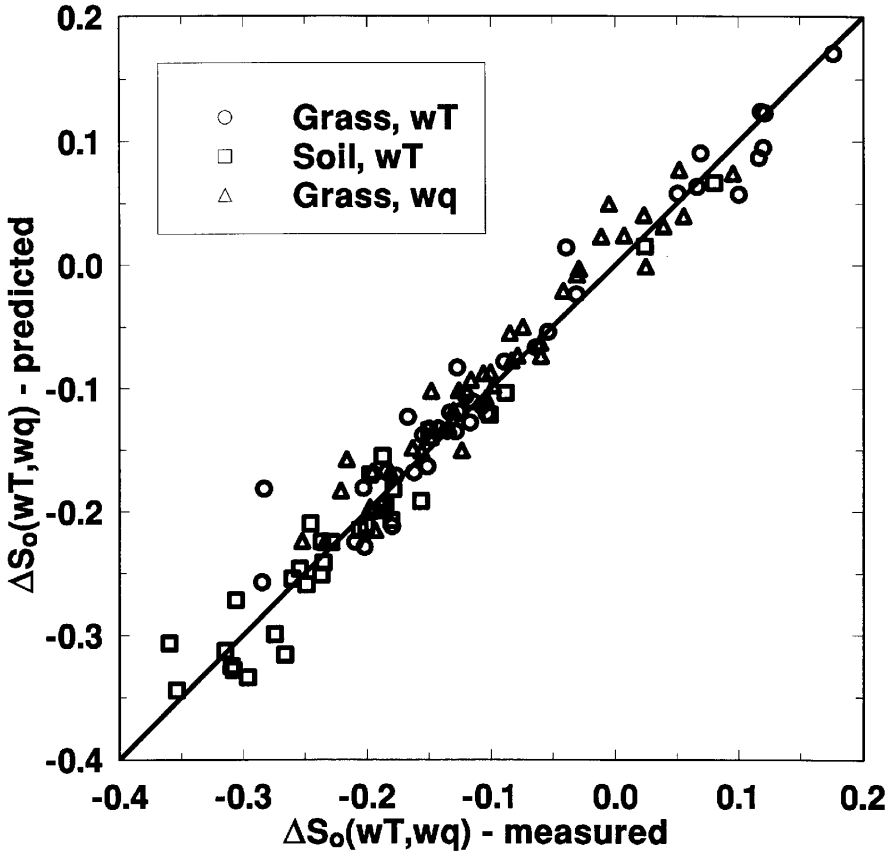

Figure 3b.

measured ΔS_0 (see definition) as well as all additive terms in Equation (3). Hence, the good agreement between measured and predicted ΔS_0 in Figure 3 may be partially biased by the fact that the measured R_{wc} is used in calculating both measured and predicted ΔS_0.

To further test the validity of CEM in scalar transport, we investigate how well this expansion describes other statistical measures such as the probability density functions (pdf) of the individual velocity and scalar time series and the flux skewness (used as a surrogate measure for the joint pdf's). The third-order CEM used by Raupach (1981), Shaw et al. (1983), Chen (1990) and others assumes that the individual pdf's of w and c can be represented by a third-order Gram-Charlier distribution. We simplified the general nth-order Gram–Charlier distribution in Nakagawa and Nezu (1977) for third cumulants to give

$$p(\hat{c}) = G(\hat{c}) \left(1 + \frac{1}{6} Q^3 (\hat{c}3 - 3\hat{c})\right),$$

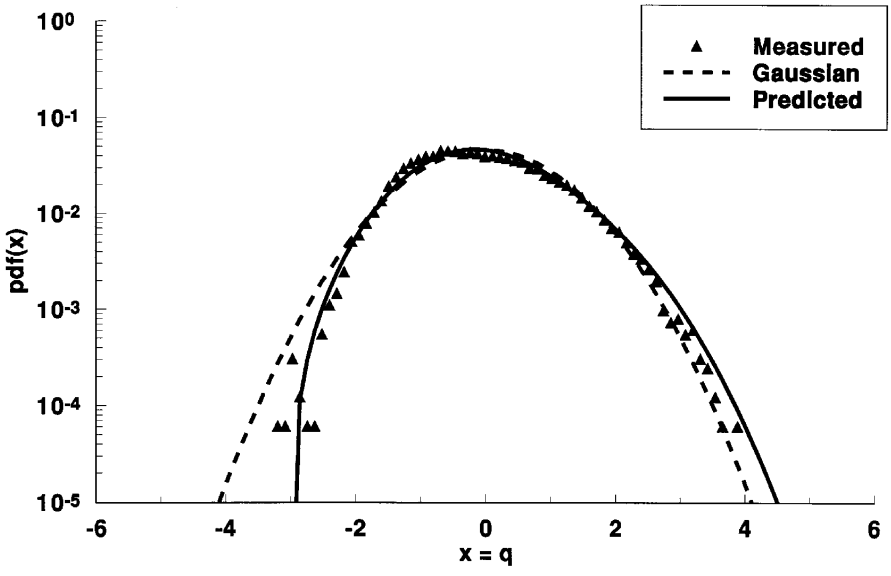

Figure 4a.

Figure 4. A comparison between measured and third-order cumulant expansion estimated pdf for (a) water vapour concentration and (b) longitudinal velocity component. The zero mean and unit variance Gaussian distribution is also shown for comparison purposes. The pdf tails are best illustrated on a semi-log scale. The atmospheric stability (z/L_{mo}) is -0.6.

$$G(\hat{c}) = \frac{1}{\sqrt{2\pi}} \exp\left(\frac{-\hat{c}^2}{2}\right), \tag{8}$$

$$\hat{c} = \frac{c}{\sigma_c}; \quad c \equiv [u, w, T, q],$$

where $G(\ )$ is a zero-mean unit variance Gaussian distribution, and $Q_3 = \langle (c/\sigma_c)^3 \rangle$ is the third cumulant of $c (= u, T,$ and $q)$ identical to the skewness. In the case of u_i, it is well recognized that the measured pdf's do not depart appreciably from $G(u_i)$ as discussed in Batchelor (1953). Thoroddsen and Van Atta (1992), Katul (1994) and Chu et al. (1996) also found that for near-neutral and slightly stable ASL flows, the w and T pdf's do not depart appreciably from Gaussian. However, for the unstable ASL, departures from Gaussian are well documented (see e.g. Maitani and Shaw, 1992) for u and T. As an illustration, a comparison between measured and third-order CEM predicted pdf's for q and u is shown in Figures 4a and 4b. The measured pdf in Figure 4 was computed as follows: (1) store the N = 16,384 data points per flow variable in vector $\tilde{A}$, (2) compute the difference between the maximum (max $\tilde{a}$) and minimum (min $\tilde{A}$) values, (3) define the bin interval to be $((\max \tilde{A} - \min \tilde{A})/100)$, and (4) carry out a frequency distribution using the resultant 100 bins. This produces a measured pdf defined for 100 discrete bin points. Good agreement between measured and third-order CEM predicted pdf

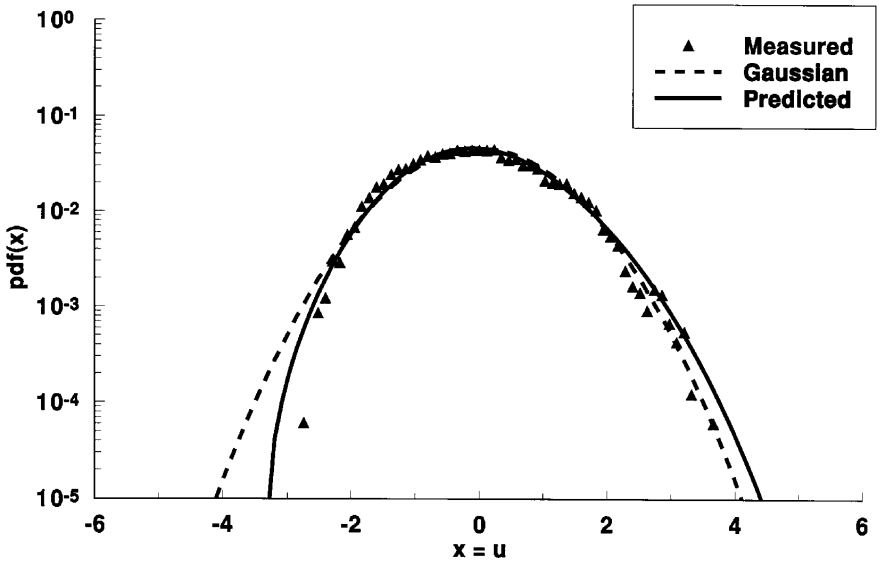

Figure 4b.

is noted in Figures 4a and 4b over three decades. Similar findings were also noted for other runs.

Rather than test the joint pdf cumulant discard predictions for each run, we use the third-order CEM to estimate the flux skewness (Q_3),

$$Q_3 = \frac{\langle (wc - \langle wc \rangle)^3 \rangle}{\sigma_{wc}^3}, \tag{9}$$

for all runs. The third-order cumulant expansion for Q_3 is

$$\begin{aligned} Q_3 \; = \; & \frac{1}{(M_{22} - R^2)^{3/2}} (M_{30}M_{03} + 9M_{12}M_{21} + 3(M_{31} + M_{13}) \\ & -2R(5R^2 - 3M_{22} + 9)), \end{aligned} \tag{10}$$

which is a modification to Nakagawa and Nezu (1977; Eq. 31) since they defined the correlation coefficient as $-\langle uw \rangle / \sigma_u \sigma_w$ while in Equation (10), $R(= +\langle wc \rangle / \sigma_w \sigma_c)$ with $c = u$, T, and q. Figures 5a and 5b compare predictions by (10) to the eddy correlation measurements in Equation (9) for momentum and scalar fluxes respectively. The performance of the third-order CEM for describing scalar and momentum transport statistics is comparable. This finding is again at variance with Chen (1990). Since the third-order CEM described ΔS_0 well, we consider whether linkages to the scalar variance budgets can be constructed in analogy to momentum (see Nakagawa and Nezu, 1977; Raupach, 1981; Nagano and Tagawa, 1988).

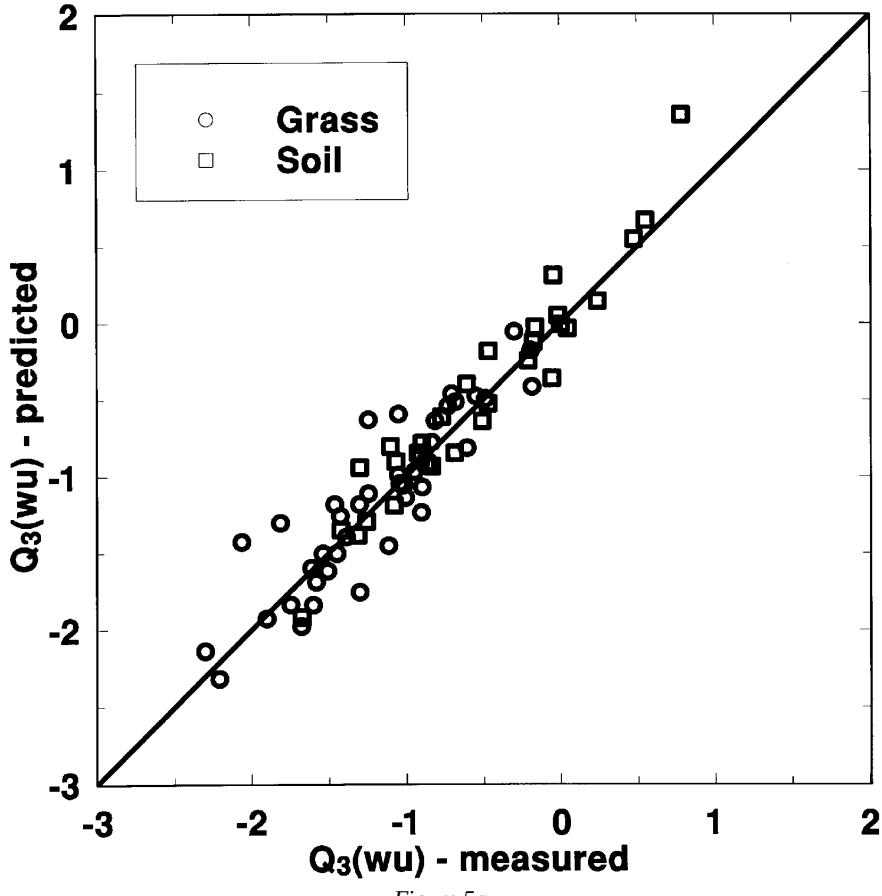

Figure 5a.

Figure 5. A comparison between measured and third-order cumulant expansion estimated (a) momentum flux skewness Q_3; (b) scalar flux skewness. The 1 : 1 line is also shown.

4.3. LINKAGES BETWEEN ΔS_0 AND SCALAR VARIANCE BUDGETS

For steady state planar homogeneous turbulence, the TKE and scalar variance budgets can be written as (Garratt, 1992)

$$0 = -\langle uw \rangle \frac{\partial \langle U \rangle}{\partial z} + \frac{g}{\langle T_a \rangle} \langle wT \rangle$$

$$- \langle \epsilon \rangle - \frac{\partial}{\partial z}(\langle wp \rangle + F_{\mathrm{TKE}}), \tag{11}$$

where

$$F_{\mathrm{TKE}} = \frac{1}{2}(\langle wu^2 \rangle + \langle wv^2 \rangle + \langle w^3 \rangle), \tag{12}$$

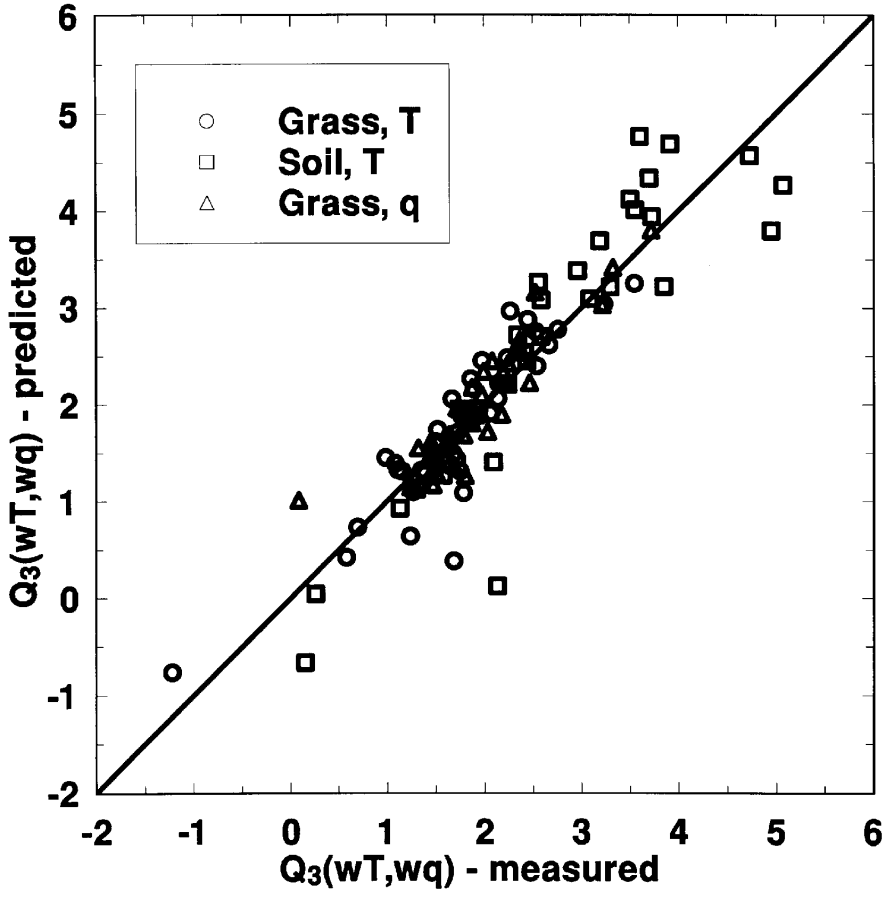

Figure 5b.

and

$$0 = -2\langle wT\rangle \frac{\partial \langle T_a\rangle}{\partial z} - 2N_T - \frac{\partial}{\partial z}\langle wT^2\rangle,$$
$$0 = -2\langle wq\rangle \frac{\partial \langle Q\rangle}{\partial z} - 2N_q - \frac{\partial}{\partial z}\langle wq^2\rangle, \tag{13}$$

where $\langle\epsilon\rangle$, N_T, and N_q are the mean TKE, temperature variance, and water vapour concentration variance dissipation rates respectively. It was shown by Nakagawa and Nezu (1977), Raupach (1981), and Shaw et al. (1983) that F_{TKE} is related to ΔS_0 using a third-order CEM. Below, we investigate whether a relationship between the flux divergence terms in (13) and ΔS_0 exists analogous to the TKE flux divergence derived in Raupach (1981). In Figure 6, this relationship between the dimensionless variance transport terms $R_{wT2} = \langle wT^2\rangle/\sigma_w\sigma_T^2$ and $R_{wq2} =$

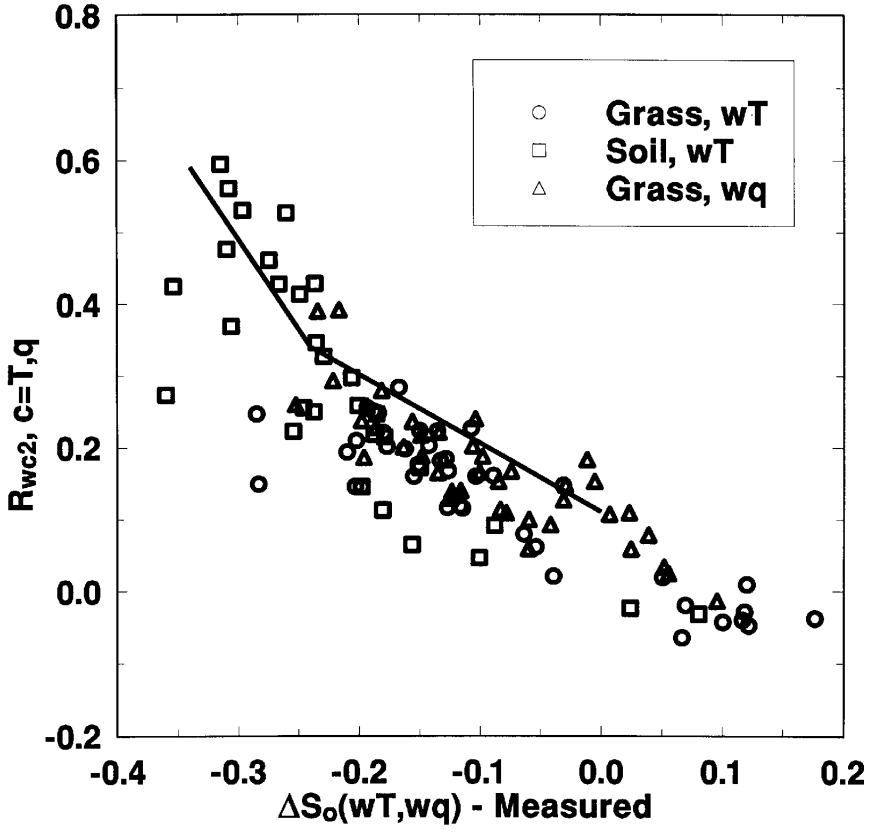

Figure 6. The relationship between eddy correlation measured R_{wT2} and R_{wq2} and ΔS_0 for temperature and water vapour at the two sites. The solid lines is an envelope estimated from similarity theory and Kader and Yaglom (1990) data.

$\langle wq^2 \rangle / \sigma_w \sigma_q^2$ and the measured ΔS_0 are shown. It is evident that ΔS_0 is, to a first approximation, related to the dimensionless variance transport term for a wide range of surface and atmospheric stability conditions.

We evaluate whether ΔS_0 and $R_{wc2} (= M_{12})$ can be derived from CEM for $c (= T, q)$ as was demonstrated for momentum by Nakagawa and Nezu (1977) and Raupach (1981). This was performed in two stages. First, we carried out a sensitivity analysis and found that setting $M_{30} - M_{03} = 0$ did not influence the performance of Equation (3) as evidenced in Table III, except for very small $|\Delta S_0|$ ($<$0.07). Hence, with this approximation, (3) reduces to

$$\Delta S_0 \approx \frac{1}{2R_{wc}\sqrt{2\pi}}(M_{21} - M_{12}). \tag{14}$$

Second, we used MOST and the extensive data set in Kader and Yaglom (1990) to establish a relationship between $R_{wc2} (= M_{12})$ and $R_{w2c} (= M_{21})$ in the dynamic

Table III

Sensitivity analysis and regression results. The third order CEM predicted $\Delta S_0^{(\mathrm{CEM}-14)}$ and $\Delta S_0^{(\mathrm{CEM}-14)}$ for scalar fluxes using Equations (3) and (14) are compared to the eddy-correlation measured $\Delta S_0^{(\mathrm{EC})}$. Equation (14) is derived from Equation (3) by setting $M_{30} - M_{03}$ to zero. The regression model is of the form: $\Delta S_0^{(\mathrm{CEM})} = A\Delta S_0^{(\mathrm{EC})} + B$. The number of runs ($n$), coefficient of determinations (R^2), and standard error of estimates (SEE) are also shown

Dependent/Independent	n	A	B	R^2	SEE
$\Delta S_0^{(\mathrm{CDM}-14)}/\Delta S_0^{(\mathrm{EC})}$	111	1.03	−0.022	0.97	0.022
$\Delta S_0^{(\mathrm{CDM}-3)}/\Delta S_0^{(\mathrm{EC})}$	111	0.97	+0.002	0.96	0.024
$\Delta S_0^{(\mathrm{CDM}-14)}/\Delta S_0^{(\mathrm{CEM}-3)}$	111	1.05	−0.026	0.98	0.017
$-0.066 < \Delta S < +0.066$	22	1.00	−0.029	0.83	0.020

(DYSL), dynamic-convective (DCSL), and free convective (FCSL) sublayers of the ASL (see also Yaglom, 1993). For these three sublayers, M_{12} and M_{21} reduce to constants given by (see Appendix A for derivation)

$$\begin{aligned} &M_{12}, M_{21} = 0.11, 0.12;\ \text{DYSL},\\ &M_{12}, M_{21} = 0.34, 0.26;\ \text{DCSL},\\ &M_{12}, M_{21} = 0.59, 0.35;\ \text{FCSL}, \end{aligned} \tag{15}$$

and with $R_{wT} = 0.5$ (see Kaimal and Finnigan, 1994 for the DCSL and FCSL), we computed ΔS_0 from Equation (14) to be on the order of

$$\begin{aligned} &\Delta S_0 \approx 0;\ \text{DYSL},\\ &\Delta S_0 \approx -0.24;\ \text{DCSL},\\ &\Delta S_0 \approx -0.34;\ \text{FCSL}. \end{aligned} \tag{16}$$

We note M_{21} and R_{wT} reverse signs when $|\Delta S_0| > 0$ since the application of Equation (14) requires that the scalar fluctuation time series be multiplied by -1 as discussed in the previous section. For very small $|\Delta S_0|$, (14) is not accurate (see Table III). The solid line in Figure 6 is a linear interpolation using Equations (15) and (16) in each of the three ASL sublayers ($c = T$ and q). The open-triangles for which $-\Delta S_0$ exceeds 0.34 are from the non-irrigated runs at Davis. Interestingly, Chen's (1990, Figure 15) data show an average $-\Delta S_0$ for temperature of 0 and 0.24 for the DYSL and DCSL respectively, and a value in excess of 0.34 for the FCSL in agreement with our measurements.

The results in Figure 6 provide a relationship between the variance budget, scalar ejections and sweeps, third-order CEM, and flux-divergence. This linkage,

given by $R_{wc2} = -0.96\Delta S_0 + 0.11$ $(-\Delta S_0 < 0.24)$ and $R_{wc2} = -2.6\Delta S_0 - 0.28$ $(-\Delta S_0 > 0.24)$ from (15) and (16), is analogous to the linkage between F_{TKE} and ΔS_0 in Nakagawa and Nezu (1977), Raupach (1981), and Shaw et al. (1983) and is much simpler than the models proposed by Nagano and Tagawa (1988, 1990, 1995). For scalar transport, it is evident that ΔS_0 changes dramatically with z as evidenced by the CSL, RSL, and ASL studies summarized in Table I; hence, our analysis shows that the flux-divergence term is large when large ΔS_0 height variations exist.

5. Conclusions

This study considered the ejection-sweep eddy motion for momentum and scalar transport in the atmospheric surface layer (ASL) above two surfaces: bare soil and tall natural grass. The following can be concluded:

1. The mean momentum ejection and sweep frequencies are comparable, constant, independent of surface roughness, and agree with other open channel measurements performed in the equilibrium region.
2. The mean scalar sweep time fraction is dependent on scalar skewness for unstable conditions while the mean scalar ejection time fraction was constant. The ejection-sweep scalar time fractions are both similar to their momentum values for near-neutral conditions confirming the similarity in scalar and momentum turbulent transport for such ASL stability conditions.
3. In contrast to a previous ASL study by Chen (1990), our study demonstrated that the third-order cumulant expansion method (CEM) predicts the individual probability density function well for velocity and scalars, the turbulent flux skewness, and the relative contribution of sweeps and ejections to the scalar flux (ΔS_0).
4. In the ASL, the measured variations in ΔS_0 $(-0.1 < \Delta S_0 \leq 0.5)$ for momentum are much larger than the values reported in laboratory studies for the equilibrium region ($\Delta S_0 \approx 0.05$).
5. Based on a sensitivity analysis, we showed that simplifications to the ΔS_0 third-order CEM scalar formulation can be applied with less than 3% accuracy loss. The simplified relation was used to link ΔS_0 to the flux-divergence term in the scalar variance budget. Based on Kader and Yaglom's (1990) three sublayer models, and their proposed formulations for the similarity functions, a relationship between ΔS_0 and the dimensionless mixed moment $\langle wc^2 \rangle / \sigma_w \sigma_c^2$ was proposed and field tested for temperature and water vapour fluctuations in the ASL.

Acknowledgments

We would like to thank Dave Petterson of the Jet Propulsion Laboratory for helping set up, maintain, and calibrate the equipment at the grass clearing; Judd Edeburn and John Sigmon for their assistance and support at the Duke Forest; and Marc Parlange, Mike Mata, Chia-Ren Chu and John Albertson for their help at the University of California, Davis Campbell Tract Facility. This project was funded, in part, by the National Science Foundation (NSF Grant No. BIR-12333), the Environmental Protection Agency (EPA) under co-operative agreement 91-0074-94 (CR817766), and the U.S. Department of Energy through the Southeast Regional Center at the University of Alabama, Tuscaloosa (DOE Cooperative Agreement No. DE-FC03-90ER61010). Portions of this work were performed at the Jet Propulsion Laboratory, California Institute of Technology under contract to the National Aeronautics and Space Administration. Funding was provided by Earth and Space Sciences Division through Barney Farmer.

Appendix A: The Magnitudes of M_{12} and M_{21} in the Three Sublayers of the ASL

The mixed moments M_{12} and M_{21} can be determined from the dimensionless similarity functions using

$$M_{21} = \frac{\phi_{w^2T}}{(\phi_w)^2\phi_T}, \qquad M_{12} = \frac{\phi_{wT^2}}{\phi_w(\phi_T)^2}, \tag{17}$$

where $\phi_w = \sigma_w/u_*$, $\phi_T = \sigma_T/T_*$, $\phi_{12} = \langle wc^2\rangle/(u_*T_*^2)$, $\phi_{21} = \langle w^2c\rangle/(u_*^2T_*)$, $M_{12} = \langle wc^2\rangle/(\sigma_w\sigma_c^2)$, $M_{21} = \langle w^2c\rangle/(\sigma_c\sigma_w^2)$, $T_* = \langle wc\rangle/u_*$, and $c = T$ or q. Kader and Yaglom (1990) determined ϕ_w, ϕ_T, ϕ_{12}, ϕ_{21} as functions of the stability parameter $\chi = -z/L_{mo}$ for the three ASL sublayers using newly acquired data from the Tsimlyansk field station as well as data from a wide range of other ASL experiments. These functions (not adjusted for the Von Karman constant) are given below:

1. Dynamic (DSAL) Sublayer ($\chi < 0.04$)

$$\begin{aligned} \phi_w &= 1.25, \\ \phi_T &= 2.90, \\ \phi_{12} &= 1.2, \\ \phi_{21} &= 0.55. \end{aligned} \tag{18}$$

2. Dynamic-Convective (DCSL) Sublayer ($0.04 < \chi < 2$)

$$\begin{aligned} \phi_w &= 1.65\chi^{1/3}, \\ \phi_T &= 1.40\chi^{1/3}, \\ \phi_{12} &= 1.0\chi^{-1/3}, \\ \phi_{21} &= 1.0\chi^{1/3}. \end{aligned} \tag{19}$$

3. Free-Convective (FCSL) Sublayer ($\chi > 2$)

$$\begin{aligned} \phi_w &= 1.35\chi^{1/3}, \\ \phi_T &= 1.55\chi^{1/3}, \\ \phi_{12} &= 1.9\chi^{-1/3}, \\ \phi_{21} &= 1.0\chi^{1/3}. \end{aligned} \tag{20}$$

Using Equations (18), (19), and (20), ΔS_0 was determined from (14) and presented in (16) assuming $\rho = 0.5$ for the DCSL and FCSL. The estimated ΔS_0, along with the estimated M_{12}, are shown as solid lines in Figure 6. These solid lines represent an envelope of possible ΔS_0 and M_{12}.

References

Albertson, J. D., Parlange, M. B., Katul, G. G., Chu, C. R., Stricker, H., and Tyler, S.: 1995, 'Sensible Heat Flux from Arid Regions: A Simple Flux-Variance Method', *Water Resour. Res.* **31**, 969–973.

Antonia, R. A. and Atkinson, J. D.: 1973, 'High-Order Moments of Reynolds Shear Stress Fluctuations in a Turbulent Boundary Layer', *J. Fluid Mech.* **58**, 581–593.

Antonia, R. A.: 1981, 'Conditional Sampling in Turbulence Measurements', *Ann. Rev. Fluid Mech.* **13**, 131–156.

Batchelor, G. K.: 1953, *The Theory of Homogeneous Turbulence*, Cambridge University Press, 210 pp.

Bergstrom, H. and Hogstrom, U.: 1989, 'Turbulent Exchange Above a Pine Forest II: Organized Structures', *Boundary-Layer Meteorol.* **49**, 231–263.

Bogard, D. G. and Tiederman, W. G.: 1987, 'Characteristics of Ejections in Turbulent Channel Flow', *J. Fluid Mech.* **179**, 1–19.

Brodkey, R. S., Wallace, J. M., and Eckelmann, H.: 1974, 'Some Properties of Truncated Signals in Bounded Shear Flows', *J. Fluid Mech.* **63**, 209–224.

Brutsaert, W.: 1982, *Evaporation into the Atmosphere: Theory, History, and Applications*, Kluwer Academic Press, 299 pp.

Cantwell, B.: 1981, 'Organized Motion in Turbulent Flow', *Ann. Rev. Fluid Mech.* **13**, 457–515.

Chen, F.: 1990, 'Turbulent Characteristics over a Rough Natural Surface Part I: Turbulent Structures', *Boundary-Layer Meteorol.* **52**, 151–175.

Chu, C. R., Parlange, M. B., Katul, G. G., and Albertson, J. D.: 1996, 'Probability Density Functions of Heat and Momentum Fluxes in the Atmospheric Surface Layer', *Water Resour. Res.* **32**, 1681–1688.

Coppin, P. A., Raupach, M. R., and Legg, B. J.: 1986, 'Experiments on Scalar Dispersion within a Model Plant Canopy Part II: An Elevated Plane Source', *Boundary-Layer Meteorol.* **35**, 167–191.

de Bruin, H. A. R., Kohsiek, W., and Van den Hurk, B. J. J. M.: 1993, 'A Verification of Some Methods to Determine the Fluxes of Momentum, Sensible Heat, and Water Vapor, Using Standard Deviation and Structure Parameter of Scalar Meteorological Quantities', *Boundary-Layer Meteorol.* **63**, 231–257.

de Bruin, H.A.R., Bink, N. I., and Kroon, L. J. M.: 1991, 'Fluxes in the Surface Layer under Advective Conditions', in T. J. Schmugge and J. C. Andre (eds.), *Workshop on Land Surface Evaporation Measurements and Parameterization*, Springer-Verlag, New York, pp. 157–169.

Finnigan, J. J.: 1985, 'Turbulent Transport in Flexible Plant Canopies', in B. A. Hutchinson and B. B. Hicks (eds.), *The Forest-Atmosphere Interaction*, D. Reidel Publishing Company, pp. 443–480.

Frenkiel, F. and Klebanoff, P.: 1967, 'Higher Order Correlations in a Turbulent Field', *Phys. Fluids* **10**, 507–520.

Frenkiel, F. and Klebanoff, P.: 1973, 'Probability Distributions and Correlations in a Turbulent Boundary Layer', *Phys. Fluids* **16**, 725–737.

Garratt, J. R.: 1978, 'Flux Profile Relations above Tall Vegetation', *Quart. J. Roy. Meteorol. Soc.* **104**, 199–211.

Garratt, J. R.: 1992, *The Atmospheric Boundary Layer*, Cambridge University Press, 316 pp.

Hsieh, C. I., Katul, G. G., Scheildge, J., Sigmon, J. T., and Knoerr, K. R.: 1996, 'Estimation of Momentum and Heat Fluxes Using Dissipation and Flux-Variance Methods in the Unstable Surface Layer', *Water Resour. Res.* **32**, 2453–2462.

Kader, B. A. and Yaglom, A. M.: 1990, 'Mean Fields and Fluctuation Moments in Unstably Stratified Turbulent Boundary Layers', *J. Fluid Mech.* **212**, 637–662.

Kaimal, J. C. and Finnigan, J. J.: 1994, *Atmospheric Boundary Layer Flows: Their Structure and Measurements*, Oxford University Press, 289 pp.

Katul, G. G. and Parlange, M. B.: 1992, 'A Penman–Brutsaert Model for Wet Surface Evaporation', *Water Resour. Res.* **28**, 121–126.

Katul, G. G.: 1994, 'A Model for Sensible Heat Flux Probability Density Function for Near-Neutral and Slightly-Stable Atmospheric Flows', *Boundary-Layer Meteorol.* **71**, 1–20.

Katul, G. G., Albertson, J. D., Parlange, M. B., Chu, C. R., and Stricker, H.: 1994a, 'Conditional Sampling, Bursting, and the Intermittent Structure of Sensible Heat Flux', *J. Geophys. Res.* **99**, 22869–22876.

Katul, G. G. and Parlange, M. B.: 1994, 'On the Active Role of Temperature in Surface Layer Turbulence', *J. Atmos. Sci.* **51**, 2181–2195.

Katul G. G., Parlange, M. B., and Chu, C. R.: 1994b, 'Intermittency, Local Isotropy, and Non-Gaussian Statistics in Atmospheric Surface Layer Turbulence', *Phys. Fluids* **6**, 2480–2492.

Katul, G. G., Goltz, S. M., Hsieh, C. I., Cheng, Y., Mowry, F., and Sigmon, J.: 1995, 'Estimation of Surface Heat and Momentum Fluxes Using the Flux-Variance Method Above Uniform and Non-uniform Terrain', *Boundary-Layer Meteorol.* **74**, 237–260.

Katul, G.G., Albertson, J. D., Hsieh, C. I., Conklin, P. S., Sigmon, J. T., Parlange, M. B., and Knoerr, K. R.: 1996, 'The Inactive Eddy-Motion and the Large Scale Turbulent Pressure Fluctuations in the Dynamic Sublayer', *J. Atmos. Sci.* **53**, 2512–2524.

Kovasznay, L. S. G., Kibens, V., and Blackwelder, R. F.: 1970, 'Large-Scale Motion in the Intermittent Region of a Turbulent Boundary Layer', *J. Fluid Mech.* **41**(2), 283–325.

Krogstad, P. A., Antonia, R. A., and Browne, L. W. B.: 1992, 'Comparison between Rough- and Smooth-Wall Turbulent Boundary Layers', *J. Fluid Mech.* **245**, 599–617.

Lloyd, C. R., Culf, A. D., Dolman, A. J., and Gash, J. H.: 1991, 'Estimates of Sensible Heat Flux from Observations of Temperature Fluctuations', *Boundary-Layer Meteorol.* **25**, 25–41.

Maitani, T. and Ohtaki, E.: 1987, 'Turbulent Transport Processes of Momentum and Sensible Heat in the Surface Layer over a Paddy Field', *Boundary-Layer Meteorol.* **40**, 283–293.

Maitani, T. and Shaw, R. H.: 1990, 'Joint Probability Analysis of Momentum and Heat Fluxes at a Deciduous Forest', *Boundary-Layer Meteorol.* **52**, 283–300.

Monin, A. S. and Obukhov, A. M.: 1954, 'Basic Laws of Turbulent Mixing in the Ground Layer of the Atmosphere', *Tr. Geofiz Inst. Akad. Nauk. S.S.S.R.* **151**, 163–187.

Monin, A. S. and Yaglom, A. M.: 1971, in J. Lumley (ed.), *Statistical Fluid Mechanics*, Vol. 1, MIT Press, 769 pp.

Nagano, Y. and Tagawa, M.: 1988, 'Statistical Characteristics of Wall Turbulence with a Passive Scalar', *J. Fluid Mech.* **196**, 157–185.

Nagano, Y. and Tagawa, M.: 1990, 'A Structural Turbulence Model for Triple Products of Velocity and Scalar', *J. Fluid Mech.* **215**, 639–657.

Nagano, Y. and Tagawa, M.: 1995, 'Coherent Motions and Heat Transfer in a Wall Turbulent Shear Flow', *J. Fluid Mech.* **305**, 127–157.
Nakagawa, H. and Nezu, I.: 1977, 'Prediction of the Contributions to the Reynolds Stress from Bursting Events in Open-Channel Flows', *J. Fluid Mech.* **80**, 99–128.
Padro, J.: 1993, 'An Investigation of Flux-Variance Methods and Universal Functions Applied to Three Land-Use Types in Unstable Conditions', *Boundary-Layer Meteorol.* **2**, 25–37.
Panofsky, H. A. and Dutton, J. A.: 1984, *Atmospheric Turbulence: Models and Methods for Engineering Applications*, John Wiley and Sons, 397 pp.
Perry, A. E., Schofield, W. H., and Joubert, P. N.: 1969, 'Rough-Wall Turbulent Boundary Layers', *J. Fluid Mech.* **37**, 383–413.
Raupach, M. R., Antonia, R. A., and Rajagopalan, S.: 1991, 'Rough-Wall Turbulent Boundary Layers', *Appl. Mech. Rev.* **44**, 1–25.
Raupach, M. R.: 1981, 'Conditional Statistics of Reynolds Stress in Rough-Wall and Smooth-Wall Turbulent Boundary Layers', *J. Fluid Mech.* **108**, 363–382.
Raupach, M. R. and Thom, A. S.: 1981, 'Turbulence in and Above Canopies', *Ann. Rev. Fluid Mech.* **13**, 97–129.
Robinson, S. K.: 1991, 'Coherent Motions in the Turbulent Boundary Layer', *Ann. Rev. Fluid Mech.* **23**, 601–639.
Shaw, R. H., Tavangar, J., and Ward, D.: 1983, 'Structure of the Reynolds Stress in a Canopy Layer', *J. Clim. Appl. Meteorol.* **22**, 1922–1931.
Shaw, R. H.: 1985, 'On Diffusive and Dispersive Fluxes in Forest Canopies', in B. A. Hutchinson and B. B. Hicks (eds.), *The Forest-Atmosphere Interaction*, D. Reidel Publishing Company, pp. 407–419.
Sorbjan, Z.: 1989, *Structure of the Atmospheric Boundary Layer*, Prentice Hall, 317 pp.
Subramanian, C. S., Rajagoplan, S., Antonia, R. A., and Chambers, A. J.: 1982, 'Comparison of Conditional Sampling and Averaging Techniques in a Turbulent Boundary Layer', *J. Fluid Mech.* **123**, 335–362.
Thoroddsen, S. T. and Van Atta, C. W.: 1992, 'Exponential Tails and Skewness of Density-Gradient Probability Functions in Stably Stratified Turbulence', *J. Fluid Mech.* **244**, 547–566.
Tillman, J. E.: 1972, 'The Indirect Determination of Stability, Heat, and Momentum Fluxes in the Atmospheric Boundary Layer from Simple Scalar Variables during Dry Unstable Conditions', *J. Appl. Meteorol.* **11**, 783–792.
Townsend, A. A.: 1976, *The Structure of Turbulent Shear Flow*, Cambridge University Press, 428 pp.
Weaver, H. L.: 1990, 'Temperature and Humidity Flux-Variance Relations Determined by One-Dimensional Eddy Correlations', *Boundary-Layer Meteorol.* **53**, 77–91.
Wesely, M. L.: 1988, 'Use of Variance Techniques to Measure Dry Air-Surface Exchange Rates', *Boundary-Layer Meteorol.* **44**, 13–31.
Willmarth, W. W. and Lu, S. S.: 1974, 'Structure of the Reynolds Stress and the Occurrence of Bursts in the Turbulent Boundary Layer', *Adv. Geophys.* **18A**, 287–314.
Wyngaard, J. C. and Sundarajan, A.: 1977, 'The Temperature Skewness Budget in the Lower Atmosphere and its Implications for Turbulence Modeling, in F. Durst, B. E. Launder, F. W. Schmidt, and J. H. Whitelaw (eds.), *Turbulent Shear Flows*, Vol. I, Springer-Verlag, pp. 319–326.
Yaglom, A. M.: 1993, 'Similarity Laws for Wall Turbulent Flows: Their Limitations and Generalizations', in *New Approaches and Concepts in Turbulence*, Monte Verita, Birkhauser Verlag Basel, pp. 7–27.